Geometry-induced textural transitions in ^{3}He-B

Tomi Ruokola

Low Temperature Laboratory, Helsinki University of Technology,

P.O. Box 2200, FIN-02015 HUT, Finland

(Dated: November 7, 2005)

Contents

I. Introduction 3

II. Setting of the problem 5

A. Textural energies 5

B. Model textures 5

III. Energy minimization 8

IV. Results 11

V. Discussion 12

References 13

I. INTRODUCTION

When a physical system is cooled, it may happen that below some critical temperature T_c the ground state of the system no longer has the full symmetry of the Hamiltonian. For instance, when a ferromagnet is cooled below the Curie temperature, it becomes spontaneously magnetized along some (in principle arbitrary) direction. This appearance of a preferred spatial direction implies the breaking of the rotational symmetry. Generally speaking, the ordered state can be described by defining an *order parameter*: a thermodynamic variable which vanishes above the transition temperature, and is nonzero below it. In the ferromagnetic example, such a quantity is provided by the magnetization vector $\mathbf{M}$ itself. Below T_c the order parameter begins to grow continuously from zero. The situation described above is an example of the so-called second order (or continuous) phase transion.

Another example of a second-order phase transition is provided by the transition of a metal to the superconducting state. However, here the symmetry breaking is of more abstract nature. The Hamiltonian of a metallic system is invariant under a transformation where the phase of all the single-particle wave functions is shifted by a constant amount ϕ: this is called *gauge symmetry*. The superconducting ground state, however, does not have this property; *i.e.* the gauge symmetry is spontaneously broken in a superconductor. This symmetry breaking gives rise to macroscopic phase coherence. The order parameter in this case can be written in the form $\Delta\, e^{i\phi}$, where the (real) magnitude Δ turns out to be related to the superconducting energy gap.

This work concentrates on the B phase of superfluid ^{3}He, which shares the phase coherence with superconductors, but also exhibits further symmetry breaking. This is due to the fact that the Cooper pairs in ^{3}He have a nontrivial internal structure, because the pairing occurs to a state with orbital angular momentum $L = 1$ and spin $S = 1$ (in superconductors the pairing state has $L = S = 0$). The Hamiltonian of liquid ^{3}He is invariant under arbitrary orbital or spin rotations. However, in the superfluid state of ^{3}He-B, there appears what is usually called *spontaneously broken spin-orbit symmetry*. This means that, even though no preferred directions exist for either the orbital or spin properties of ^{3}He-B, the relative orientation between the orbital and spin degrees of freedom of the pairing state becomes fixed (for details, see [1]). Therefore, any anisotropy induced for the spin properties (by *e.g.* an external magnetic field) leads to orbital anisotropy as well, and vice versa.

The two broken symmetries of ^{3}He-B combine into an order parameter of the form [2]

$$\Psi = \Delta e^{i\phi} \mathbf{R}(\hat{\mathbf{n}}, \theta), \tag{1}$$

where $\mathbf{R} = \mathbf{R}(\hat{\mathbf{n}}, \theta)$ is a real 3D rotation matrix (describing the relative orientation discussed above): $\hat{\mathbf{n}}$ is the axis of rotation and θ is the rotation angle. With respect to the pairing interaction, all values of $\hat{\mathbf{n}}$ and θ are energetically degenerate; however, this degeneracy is lifted by considering the weaker interactions present in the system. The small dipole–dipole interaction between the ^{3}He nuclei fixes $\theta_{\mathrm{L}} = \arccos(-\frac{1}{4}) \approx 104°$, but is still degenerate with respect to the vector $\hat{\mathbf{n}}$. The orientation of $\hat{\mathbf{n}}$ is subject to further, still weaker interactions, imposed by *e.g.* external electric and magnetic fields, the surfaces of the container, and the flow of the fluid. Generally speaking, these orienting influences are spatially inhomogeneous, giving rise to spatially varying vector fields $\hat{\mathbf{n}}(\mathbf{r})$ known as *textures*.

The textures in ^{3}He-B can be very extended: the characteristic length scales are of the order of the typical container dimensions. Therefore, the boundary conditions are important in many contexts. At solid boundaries, and in the presence of a strong external magnetic field $\mathbf{H}$ (as in NMR experiments), the unit vector $\hat{\mathbf{l}}$, defined as

$$\hat{\mathbf{l}} \equiv \mathbf{R}(\hat{\mathbf{n}}, \theta_{\mathrm{L}}) \cdot \mathbf{H}/H, \tag{2}$$

tends to be oriented perpendicular to the boundary, $\hat{\mathbf{l}} \parallel \hat{\mathbf{s}}$, where $\hat{\mathbf{s}}$ is the surface normal. In a cylindrical container, the order-parameter textures resulting from these boundary conditions are typically found to be axisymmetric, of the so-called *flare-out* form.

However, in certain situations different boundary conditions may arise. For example, it is well established that $\hat{\mathbf{l}} \perp \hat{\mathbf{s}}$ is the preferred alignment at the boundary separating the A and B phases of ^{3}He [3]. This can be realized in experiments where the two phases are stabilized on top of each other with the help of a magnetic field gradient (see for instance [4]). In particular, new experiments planned to simulate a black hole event horizon with superfluid helium [5] require a thin layer of B phase; such restricted geometry might emphasize the role of the modified boundary condition. Also, recent experiments of ^{3}He-B in aerogel suggest that the $\hat{\mathbf{l}} \perp \hat{\mathbf{s}}$ orientation is favored at the boundary separating the fluid immersed in aerogel from bulk ^{3}He-B [6]. The purpose of this work is to study whether, in cylindrical geometry, such modified boundary conditions can give rise to *nonaxisymmetric* textures deviating from the standard flare-out form.

II. SETTING OF THE PROBLEM

A. Textural energies

As stated in the Introduction, there are several forces influencing the orientation of the $\hat{\mathbf{n}}$ vector field. In this work we consider the case of a stationary fluid under a constant external magnetic field $\mathbf{H}$. Then, the leading terms in the Taylor expansion of the free energy of the texture are [7]:

i) bulk field energy

$$F^{\mathrm{H}} = -a \int d^3r \, (\mathbf{H} \cdot \hat{\mathbf{n}})^2 \tag{3}$$

ii) surface dipole energy

$$F^{\mathrm{D}} = -b \int d^2r (\hat{\mathbf{s}} \cdot \hat{\mathbf{n}})^2 \tag{4}$$

iii) bending energy

$$\begin{aligned} F^{\mathrm{B}} = \frac{c}{13} \int d^3r \Big[& 16[\hat{\mathbf{n}} \times (\nabla \times \hat{\mathbf{n}})]^2 + 13(\nabla \cdot \hat{\mathbf{n}})^2 + 11(\hat{\mathbf{n}} \cdot \nabla \times \hat{\mathbf{n}})^2 \\ & -2\sqrt{15}(\nabla \cdot \hat{\mathbf{n}})(\hat{\mathbf{n}} \cdot \nabla \times \hat{\mathbf{n}}) + 16\nabla \cdot [(\hat{\mathbf{n}} \cdot \nabla)\hat{\mathbf{n}} - \hat{\mathbf{n}}(\nabla \cdot \hat{\mathbf{n}})] \Big] \end{aligned} \tag{5}$$

iv) surface field energy

$$F^{\mathrm{S}} = -d \int d^2r \, H^2 (\hat{\mathbf{s}} \cdot \hat{\mathbf{l}})^2 \tag{6}$$

where a, b, c, and d are expansion coefficients. We assume that $b \ll dH^2$, so that we can neglect F^{D} from our calculation; this happens when $H \gg H_D$, with the dipole field $H_D \approx 2\,\mathrm{mT}$ [2]. This condition is satisfied in the presence of typical NMR fields. Furthermore, we will also omit the term F^{H} for simplicity, because we wish to concentrate on the effect of the boundary conditions in restricted geometries. The texture problem then requires finding the vector field $\hat{\mathbf{n}}(\mathbf{r})$ which minimizes the total free energy $F^{\mathrm{B}} + F^{\mathrm{S}}$.

B. Model textures

When written in the form of Eq. (6), the ordinary perpendicular orientation of $\hat{\mathbf{l}}$ at the surface corresponds to $d > 0$ and parallel orientation corresponds to $d < 0$. To examine different situations, we consider a cylinder (radius R, height h) with $d = d_1$ at the bottom and side surfaces, and $d = d_2$ at the top surface (Fig. 1). Here d_1 and d_2 are arbitrary real numbers, so that $d_1 = d_2 > 0$ corresponds to a standard case of a container with ordinary

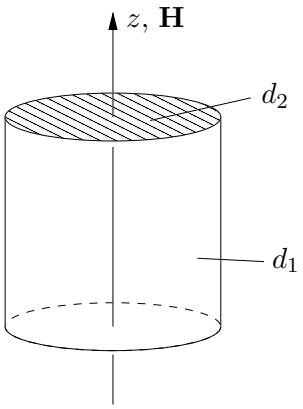

FIG. 1: We investigate the textures of superfluid ^{3}He in a cylinder and in an axial magnetic field **H**. We allow the different surfaces of the cylinder to have different surface energy coefficients; d_1 on the bottom and the sides and d_2 on the top.

solid surfaces, $d_1 = d_2 < 0$ could *e.g.* model a container filled with aerogel (see the end of Introduction above), and $d_1 > 0,\ d_2 < 0$ refers to a case where the B phase volume borders to A phase on the top. The cylinder axis and the magnetic field are taken to be aligned in the z direction.

The general problem of finding the texture $\hat{\mathbf{n}}(\mathbf{r})$ which minimizes the total free energy $F^{\rm B}+F^{\rm S}$ is a very difficult task. Therefore, we proceed by using simple but plausible trial forms for different types of textures. First, if $d_1,\ d_2 > 0$, then $\hat{\mathbf{l}}$ tends to be oriented everywhere perpendicular to the walls. Clearly, it is impossible to satisfy this requirement everywhere in the cylinder, but a simple and reasonable ansatz can be obtained with the following *radial texture*

$$\begin{aligned} l_r &= \tanh\, \alpha\rho \\ l_\theta &= 0 \\ l_z &= \mathrm{sech}\, \alpha\rho, \end{aligned} \tag{7}$$

where ρ is the normalized radial coordinate, $\rho = r/R$, and α is a variational parameter. If $d_2 < 0$, Eq. (7) still presents a reasonable solution if α is large. Of course, for $d_1 > 0$, $d_2 < 0$ the preferred orientation is $\hat{\mathbf{l}} \parallel \hat{\mathbf{s}}$ on the bottom surface and $\hat{\mathbf{l}} \perp \hat{\mathbf{s}}$ on the top surface but to facilitate this we would need z-dependent trial functions. However, for simplicity, we use functions with only a radial dependence.

If $d_1 < 0$, the preferred alignment on the side walls is $\hat{\mathbf{l}} \perp \hat{\mathbf{s}}$, and we choose as a trial

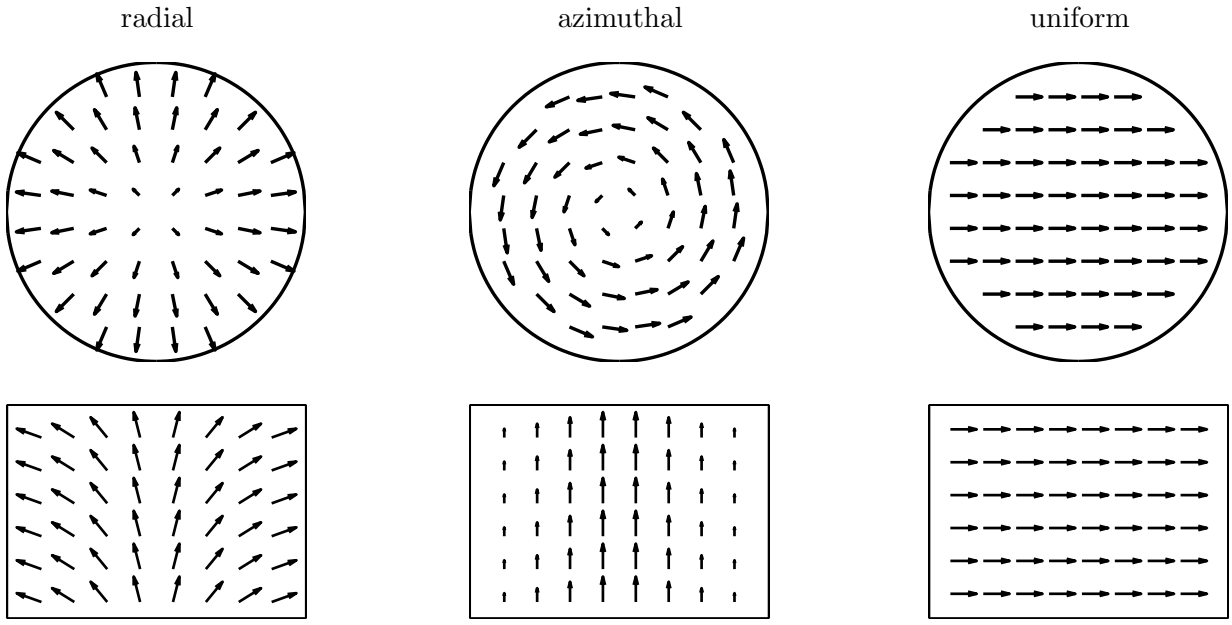

$\hat{\mathbf{l}} = \tanh \alpha\rho\, \hat{\mathbf{r}} + \operatorname{sech} \alpha\rho\, \hat{\mathbf{z}}$	$\hat{\mathbf{l}} = \tanh \alpha\rho\, \hat{\boldsymbol{\theta}} + \operatorname{sech} \alpha\rho\, \hat{\mathbf{z}}$	$\hat{\mathbf{l}} = \hat{\mathbf{x}}$

TABLE I: The three trial textures. The upper figures show the $\hat{\mathbf{l}}$ field viewed from the top of the cylinder and the lower figures show the field at $y = 0$ viewed from the side.

function the *azimuthal texture*

$$\begin{aligned} l_r &= 0 \\ l_\theta &= \tanh\, \alpha\rho \\ l_z &= \operatorname{sech}\, \alpha\rho \end{aligned} \tag{8}$$

Both of the textures above are axisymmetric. However, if the size of the cylinder is reduced below a certain limit, it is conceivable that the bending energy starts to dominate the surface energy, and thus it is advantageous to have the texture more uniform; for this purpose we introduce the simple *uniform texture*

$$\hat{\mathbf{l}} = \hat{\mathbf{x}}. \tag{9}$$

Note that $\hat{\mathbf{l}} = \cos\beta\hat{\mathbf{x}} + \sin\beta\hat{\mathbf{z}}$ (with β a variational parameter) would be a more generic uniform texture but we show below that the energy minimum occurs only for $\hat{\mathbf{l}} = \hat{\mathbf{x}}$ ($\beta = 0$) or $\hat{\mathbf{l}} = \hat{\mathbf{z}}$ ($\beta = \pi/2$), and the latter case is implicitly contained in Eqs. (7) and (8) with $\alpha = 0$.

III. ENERGY MINIMIZATION

Let us start by calculating the free energy for the uniform texture. Naturally the contribution from the bending energy is zero; for the surface energy, we use for the moment the more generic texture

$$\hat{\mathbf{l}} = \cos\beta\,\hat{\mathbf{x}} + \sin\beta\,\hat{\mathbf{z}} \tag{10}$$

or

$$\hat{\mathbf{l}} = \cos\beta\cos\theta\,\hat{\mathbf{r}} - \cos\beta\sin\theta\,\hat{\boldsymbol{\theta}} + \sin\beta\,\hat{\mathbf{z}}. \tag{11}$$

For our cylindrical textures, the surface energy Eq. (6) reads

$$F^{\mathrm{S}} = -4\pi R^2\bar{d}H^2\int_0^1 \rho l_z(\rho)^2 d\rho - Rhd_1H^2\int_0^{2\pi} l_r(\rho=1,\theta)^2 d\theta, \tag{12}$$

where $\bar{d} \equiv \frac{1}{2}(d_1+d_2)$. Now, inserting Eq. (11) into Eq. (12) yields

$$F^{\mathrm{S}}_{\mathrm{uni}} = -\pi RH^2(hd_1\cos^2\beta + 2R\bar{d}\sin^2\beta). \tag{13}$$

This is minimized when $\beta = 0$ or $\beta = \pi/2$, and as noted above, the latter case is included in the radial and azimuthal textures; therefore we choose $\beta = 0$ with no loss of generality, and the total free energy for the uniform texture $\hat{\mathbf{l}} = \hat{\mathbf{x}}$ is

$$F_{\mathrm{uni}} = -\pi Rhd_1H^2. \tag{14}$$

The surface energy for the radial texture is obtained by inserting Eq. (7) into Eq. (12), yielding

$$F^{\mathrm{S}}_{\mathrm{rad}} = -4\pi R^2\bar{d}H^2 f_1(\alpha) - 2\pi Rhd_1H^2\tanh^2\alpha, \tag{15}$$

with

$$\begin{aligned} f_1(\alpha) &= \int_0^1 \rho\,\mathrm{sech}^2\,\alpha\rho\; d\rho \\ &= -\frac{\log\cosh\alpha}{\alpha^2} + \frac{\tanh\alpha}{\alpha}. \end{aligned} \tag{16}$$

Similarly, Eqs. (8) and (12) give the surface energy for the azimuthal texture as

$$F^{\mathrm{S}}_{\mathrm{azi}} = -4\pi R^2\bar{d}H^2 f_1(\alpha) \tag{17}$$

The bending energy of Eq. (5) can be expressed for a cylindrical volume as

$$F^{\mathrm{B}} = \frac{2\pi ch}{13} f_2(\alpha) \tag{18}$$

where

$$f_2(\alpha) = \int_0^1 \rho \Big[16[\hat{\mathbf{n}} \times (\nabla \times \hat{\mathbf{n}})]^2 + 13(\nabla \cdot \hat{\mathbf{n}})^2 + 11(\hat{\mathbf{n}} \cdot \nabla \times \hat{\mathbf{n}})^2 \\ -2\sqrt{15}(\nabla \cdot \hat{\mathbf{n}})(\hat{\mathbf{n}} \cdot \nabla \times \hat{\mathbf{n}}) + 16\nabla \cdot [(\hat{\mathbf{n}} \cdot \nabla)\hat{\mathbf{n}} - \hat{\mathbf{n}}(\nabla \cdot \hat{\mathbf{n}})]\Big]\, d\rho. \tag{19}$$

In this form, the dimensionless differential operators have R as the unit of length.

To calculate f_2, we must express the texture in terms of $\hat{\mathbf{n}}$ instead of $\hat{\mathbf{l}}$. Because the magnetic field is oriented in the z direction, we have $\hat{\mathbf{l}} = \mathbf{R}(\hat{\mathbf{n}}, \theta_{\mathrm{L}}) \cdot \hat{\mathbf{z}}$, and an analytic expression for the rotation matrix gives [8]

$$\hat{\mathbf{l}} = \hat{\mathbf{z}} \cos\theta_{\mathrm{L}} + \hat{\mathbf{n}}(\hat{\mathbf{n}} \cdot \hat{\mathbf{z}})(1 - \cos\theta_{\mathrm{L}}) - (\hat{\mathbf{z}} \times \hat{\mathbf{n}}) \sin\theta_{\mathrm{L}} \tag{20}$$

which can be solved for $\hat{\mathbf{n}}$ (using $\cos\theta_{\mathrm{L}} = -1/4$) as

$$\begin{aligned} n_r &= \frac{1}{\sqrt{5}} \frac{-\sqrt{3} l_\theta \pm l_r \sqrt{4l_z + 1}}{l_z + 1} \\ n_\theta &= \frac{1}{\sqrt{5}} \frac{\sqrt{3} l_r \pm l_\theta \sqrt{4l_z + 1}}{l_z + 1} \\ n_z &= \pm \frac{1}{\sqrt{5}} \sqrt{4l_z + 1} \end{aligned} \tag{21}$$

The solution is doubly degenerate, i.e., one must choose either the upper or lower signs in all equations; here we choose the upper ones. Then, combining Eqs. (7) and (21) gives the radial texture:

$$\begin{aligned} n_r &= \frac{\sinh\alpha\rho \sqrt{1 + 4\,\mathrm{sech}\,\alpha\rho}}{\sqrt{5}(1 + \cosh\alpha\rho)} \\ n_\theta &= \frac{\sqrt{3}\sinh\alpha\rho}{\sqrt{5}(1 + \cosh\alpha\rho)} \\ n_z &= \frac{\sqrt{1 + 4\,\mathrm{sech}\,\alpha\rho}}{\sqrt{5}}, \end{aligned} \tag{22}$$

and Eqs. (8) and (21) the azimuthal texture:

$$\begin{aligned} n_r &= -\frac{\sqrt{3}\sinh\alpha\rho}{\sqrt{5}(1 + \cosh\alpha\rho)} \\ n_\theta &= \frac{\sinh\alpha\rho \sqrt{1 + 4\,\mathrm{sech}\,\alpha\rho}}{\sqrt{5}(1 + \cosh\alpha\rho)} \\ n_z &= \frac{\sqrt{1 + 4\,\mathrm{sech}\,\alpha\rho}}{\sqrt{5}}. \end{aligned} \tag{23}$$

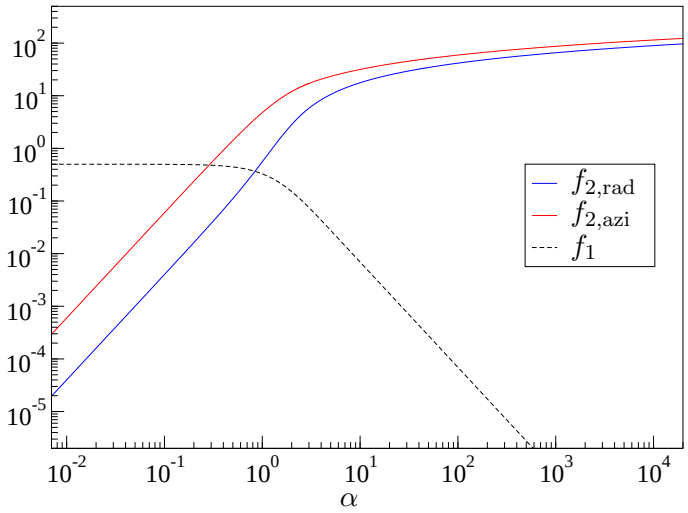

FIG. 2: A plot of the functions f_1 and f_2, given by Eqs. (16) and (19), for the radial and azimuthal textures.

Clearly, the integral in Eq. (19) resulting from these $\hat{\mathbf{n}}$ vector fields is too complicated to be calculated analytically, and we must resort to numerical computation; the obtained values of f_2 for the two textures are plotted in Fig. 2.

Now, the free energies for all three textures, $F_i = F_i^{\mathrm{S}} + F_i^{\mathrm{B}}$, from Eqs. (14), (15), (17) and (18), can be conveniently expressed as

$$F_i = -4\pi R^2 H^2 |\bar{d}| \max_{\alpha} g_i(u, v, \alpha) \tag{24}$$

with the function g_i for the different textures given by

$$g_{\mathrm{rad}}(u, v, \alpha) = \frac{u}{|u|}\Big[f_1(\alpha) - \frac{1}{26u} f_{2,\mathrm{rad}}(\alpha) + \frac{1}{2} v \tanh^2 \alpha\Big] \tag{25}$$

$$g_{\mathrm{azi}}(u, \alpha) = \frac{u}{|u|}\Big[f_1(\alpha) - \frac{1}{26u} f_{2,\mathrm{azi}}(\alpha)\Big] \tag{26}$$

$$g_{\mathrm{uni}}(u, v) = \frac{u}{|u|}\frac{v}{4} \tag{27}$$

where we have introduced the dimensionless parameters

$$u = \frac{\bar{d} H^2 R^2}{ch}, \quad v = \frac{h d_1}{R\bar{d}} \tag{28}$$

For given values of u and v, we will seek the maximum of g_{rad} and g_{azi} with respect to α numerically and compare the outcome with g_{uni}. The largest of these three g values corresponds to the minimum energy texture as per Eq. (24); the resulting phase diagram in

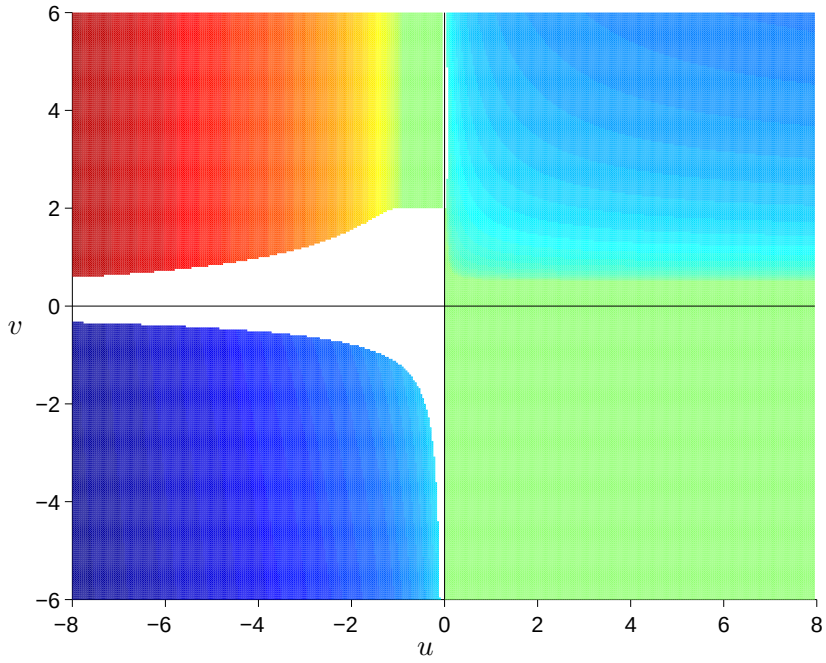

FIG. 3: The phase diagram in u–v plane. White color indicates the uniform texture $\hat{\mathbf{l}} = \hat{\mathbf{x}}$, red is the radial texture (darker red corresponds to larger α) and blue is the azimuthal texture (darker blue corresponds to larger α). Green is a uniform texture along the z axis ($\alpha = 0$).

u–v space is shown in Fig. 3. Solving Eq. (28) for R and h gives

$$R = \frac{c}{d_1 H^2}\, uv, \quad h = \frac{c\bar{d}}{d_1^2 H^2}\, uv^2 \tag{29}$$

Using this transformation, Fig. 4 gives the phase diagram in R–h space.

IV. RESULTS

According to Eq. (29), the natural unit for the cylinder radius is c/d_1H^2 and for the height $c\bar{d}/d_1^2H^2$. Since we can have $d_1, d_2 < 0$, also R and h expressed in these units can be negative, and therefore the phase diagram in Fig. 4 spans the whole plane. Let us examine this graph one quadrant at a time.

In the first quadrant we have $d_1 > 0$ and $d_1 + d_2 > 0$. This implies either $d_2 > 0$, or if $d_2 < 0$, we must have $|d_2| < |d_1|$. The former corresponds to a container with ordinary boundary, the latter has an AB boundary at the top. We notice that we can have uniform texture whenever R is small enough, $R < 0.34\ c/d_1H^2$.

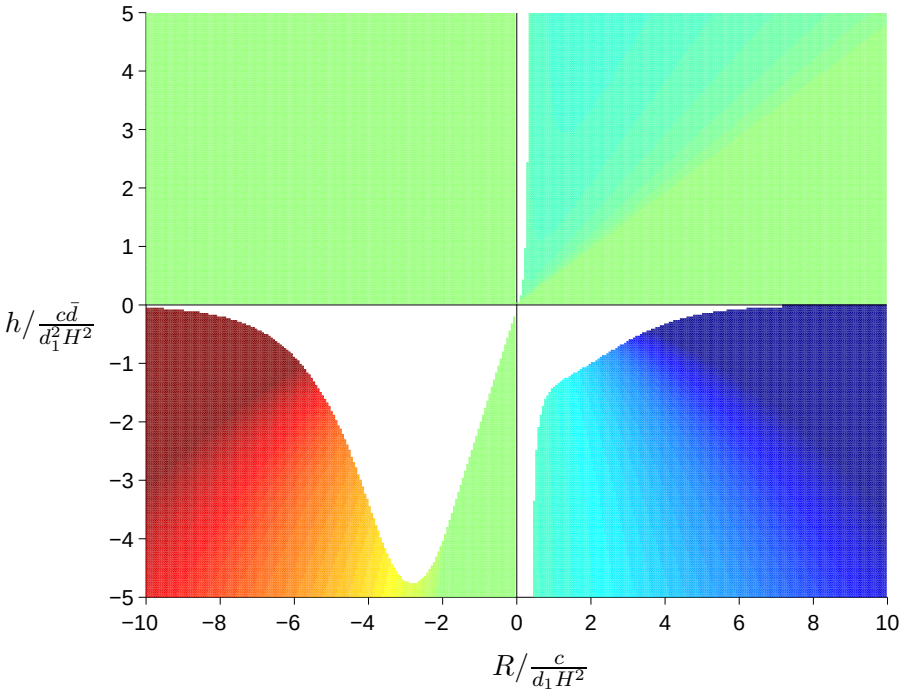

FIG. 4: The phase diagram in R–h plane. Colors as in Fig. 3.

The second quadrant has $d_1 < 0$ and $d_2 > 0$. At the moment there does not seem to be any experimental realization of these boundary conditions. In addition, the phase diagram for this region is rather uninteresting, containing only the trivial axisymmetric texture $\hat{\mathbf{l}} = \hat{\mathbf{z}}$.

In the third quadrant we have $d_1 < 0$ and $d_1 + d_2 < 0$, where the case $d_1, d_2 < 0$ corresponds to the tentative identification for a container filled with aerogel. Notice that a uniform texture can here be realized over a considerable region of parameters in the range with $h < 4.8|c/d_1H^2|$.

Finally, the fourth quadrant has $d_1 > 0$ and $d_2 < 0$, corresponding to a situation with a cylinder containing an AB boundary (note that the AB boundary case lies either in the first or fourth quadrant, depending on whether $|d_2| < |d_1|$ or $|d_2| > |d_1|$). Here we also have a uniform texture in a region approximately defined by $h/|c/d_1H^2| < 1.8 - 0.4R/(c/d_1H^2)$, as well as with small radii, $R < 0.34\ c/d_1H^2$.

V. DISCUSSION

In this work, we have studied the effect of modified boundary conditions on textural symmetries in ^{3}He-B contained in a cylinder, and in the presence of an axial magnetic field.

In particular, we wanted to study whether these modifications can lead to the realization of nonaxisymmetric textures. We have found that such a situation can indeed be realized if the dimensions of the containing cylinder are small enough. To estimate these limiting values, and the experimental relevance, we need to approximate the values for the length scales

$$L_R = \left| \frac{c}{d_1 H^2} \right|, \qquad L_h = \left| \frac{c\bar{d}}{d_1^2 H^2} \right| = L_R \left| \frac{\bar{d}}{d_1} \right| \tag{30}$$

The coefficients c and d are given in the Ginzburg–Landau approximation as [2, 7]

$$c_{\mathrm{GL}} = \frac{13\,\hbar^2}{32\,m^*} \rho\,(1 - T/T_c) \tag{31}$$

$$d_{\mathrm{GL}} = \tfrac{8}{3} \xi_0 \chi_N\,(1 - T/T_c)^{1/2} \tag{32}$$

where m^* is the effective mass, ρ the total fluid density, ξ_0 the zero-temperature coherence length, and χ_N the normal fluid susceptibility. Then we have a characteristic length for $T \to T_c$ as

$$L \equiv \frac{c_{\mathrm{GL}}}{d_{\mathrm{GL}} H^2} = L_0\,\frac{(1 - T/T_c)^{1/2}}{(H/H_D)^2} \tag{33}$$

with $L_0 \approx 2$ cm and $H_D \approx 2$ mT. Remember that we assumed that $H \gg H_D$; however, even with $H/H_D \approx 4$ the characteristic dimension is in the millimeter range. The value of d_{GL} in Eq. (32) has been calculated for specularly reflecting solid surfaces, but it is reasonable to assume that both for the aerogel and the A–B boundary the value of the coefficient is $d = -C\,d_{\mathrm{GL}}$, where C is a constant of the order of unity. Thus, we conclude that our estimations indicate that nonaxisymmetric order-parameter textures could be realized in experimentally feasible situations, provided that the boundary conditions are modified in the assumed manner. A quantitative study, however, would have to involve solving the full 3D texture problem numerically, including the bulk contribution of Eq. (3).

---

[1] A. J. Leggett, Rev. Mod. Phys. **47**, 331 (1975).

[2] D. Vollhardt and P. Wölfle, *The superfluid phases of helium 3* (Taylor & Francis, 1990).

[3] E. V. Thuneberg, Phys. Rev. B **44**, 9685 (1991).

[4] R. Blaauwgeers, V. B. Eltsov, G. Eska, A. P. Finne, R. P. Haley, M. Krusius, J. J. Ruohio, L. Skrbek, and G. E. Volovik, Phys. Rev. Lett. **89**, 155301 (2002).

[5] G. E. Volovik, JETP Lett. **76**, 240 (2002).

[6] V. V. Dmitriev, N. Mulders, V. V. Zavjalov, and D. E. Zmeeva, to be published in LT24 Proceedings.

[7] H. Smith, W. F. Brinkman, and S. Engelsberg, Phys. Rev. B **15**, 199 (1977).

[8] E. W. Weisstein (2005), URL `http://mathworld.wolfram.com/RotationMatrix.html`.